Research Article | Vol. 26, No. 21 | 15 Oct 2018 | OPTICS EXPRESS 27089
Optics EXPRESS

Mechanisms of perfect absorption in nano-composite systems

SEBASTIAN MADER[1,*] AND OLIVIER J.F. MARTIN[1,2]

[1]*Nanophotonics and Metrology Laboratory, Swiss Federal Institute of Technology Lausanne (EPFL), Station 1, 1015 Lausanne, Switzerland*
[2]*olivier.martin@epfl.ch*
**sebastian.mader@epfl.ch*

Abstract: Recently, it was noted that losses in plasmonics can also enable several useful optical functionalities. One class of structures that can maximize absorption are metal insulator metal systems. Here, we study 3-layer systems with a nano-composite metal layer as top layer. These systems can absorb almost 100% of light at visible frequencies, even though they contain only dielectrics and highly reflecting metals. We elucidate the underlying physical phenomenon that leads to this extraordinary high and broadband absorption. A comprehensive study of the particle material and shape, mirror material and dielectric spacer thickness is provided to identify their influence on the overall absorption. Thus, we can provide detailed design guidelines for realizing optical functionalities that require near-perfect absorption over specific wavelength bands. Our results reveal the strong role of lossy Fabry-Perot interference within these systems despite their thickness being well below half a wavelength.

1. Introduction

For decades, losses associated with plasmonics were seen as detrimental; however, it was recently noted that losses can also enable several useful optical functionalities and are also related to strong local field enhancements [1]. Thus, they can assist one in improving the performance of various applications including solar power [2] and sensing [3], e.g. Raman scattering [4]. One particular class of structures that can maximize absorption in the visible spectrum (VIS) are metal insulator metal (MIM) systems [5]. Such 3-layer systems consist typically of a metallic base layer (mirror layer), a dielectric spacer layer and an at least partially metallic top layer. Although, dielectric top layers are also explored to maximize absorption bandwidth and strength [6].

Several well-ordered and defined MIMs have been manufactured [7–14]. They have typically periodic top layers and can achieve broad-band absorption levels in the range of 60-80% for the case of thoroughly optimized systems [7], while certain systems can even absorb up to 100% in the infrared spectrum [8]. The periodicity and the generally well-defined geometry assists analysis, including their dipolar and quadrupolar resonances [9]. It is also possible to quantitatively study the coupling of the localized surface plasmon (LSP) mode of the individual nanostructures with the surface plasmon polariton (SPP) of the metallic mirror layer [10]. Recently, MIMs were proposed that are oriented vertically and can even reach nearly 100% absorption over a broad spectrum [11]. All these well-ordered structures require however high precision manufacturing processes, such as ebeam lithography, which limits manufacturing throughput and structured area size. Additionally, the achievable maximum absorption and bandwidth of periodic systems is limited compared to systems where at least one layer contains random elements. Typically, the top layer contains randomly sized and arranged metal nano particles that are usually embedded in a dielectric matrix (in this article we will call such a layer a nano-composite layer).

#342424 https://doi.org/10.1364/OE.26.027089
Journal © 2018 Received 20 Aug 2018; revised 21 Sep 2018; accepted 21 Sep 2018; published 2 Oct 2018

Optics EXPRESS

Nano-composite layers can be created by direct thin layer evaporation [15–18], thermal annealing [19–21], laser-induced dewetting [22], co-evaporation [23–26], spin-coating [27] or even through simple drop-casting [28]. The MIM realization of Hedayati et al. in 2011 exceeded 95% absorption across the entire VIS, thus realizing a very strong and broad absorbing MIM system with a relatively simple and scalable co-evaporation technique of gold and SiO_2, which produces a gold nano-composite layer [25]. Contrary to the needs for high precision machining of periodic systems, in this approach one must only control two evaporation rates. A similar optical performance was observed for gold, silver and copper based nano-composites [29].

It is fascinating that a system consisting only of transparent and highly reflective materials can absorb almost 100% of the incident light and the objective of this paper is to elucidate the underlying physical phenomenon.

The random nature and nanometer dimensions of the composite layer obscure an insightful analytical analysis of the system's optical properties that lead to this performance. Thus, other authors resorted to studying this system numerically using finite difference time domain (FDTD) algorithms [30,31]. Etrich et al. focused on retrieving the optical parameters of the nano-composite layer through simulations and optimized the dielectric spacer thickness to enhance absorption [30]. This optimization was carried out with a transfer matrix algorithm, which results agreed very well with those obtained by FDTD. Feng et al. researched the optical parameters required to achieve high and broadband absorption [31]. They identified for example that perfect absorbers require a dielectric spacer layer at least 20 nm thick to assure modest requirements on the nano-composite layer permittivity.

Both research groups treated the metallic nano-composite layer as a homogenous, dispersive and isotropic material and focused on its "macroscopic" properties. In contrast, we focus here on understanding the microscopic absorption mechanisms of the system described in [25], which was not undertaken yet to the best of our knowledge. In particular, we address the question of the broad bandwidth light absorption and where it is absorbed locally. Possible resonance broadening mechanisms associated with variations of the gold particles shape, size, position or plasmonic coupling to the metal mirror were suggested in [25,29]; however, we rule out that latter mechanism, as discussed in Section 3. Instead we propose that the resonance broadening effect is based on lossy Fabry-Perot interferences in combination with plasmonic inter-particle coupling.

The paper is organized as follows: Section 2 describes the simulation model used; the optical response of single particles at some distances above a mirror layer is discussed in Section 3; while the response of many particle systems is discussed in Section 4, followed by a conclusion.

2. Simulation methodology

Lumerical FDTD, a commercial-grade simulator based on the FDTD method is used to perform all simulations below [32]. Figure 1 shows the general simulation layout used here. It consists of a linear polarized light source in the x-z-plane, a metallic nano-composite layer, a dielectric spacer layer and a mirror layer. This MIM structure is embedded in a lossless dielectric background of constant refractive index 1.5. Plane waves first impinge on the nano-composite layer before they pass the dielectric spacer layer and then hit the 100 nm thick metallic mirror layer. Bloch-type periodic boundary conditions have been used and power detectors were placed at appropriate positions.

Optics EXPRESS

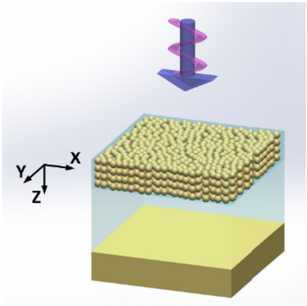

Fig. 1. Visualization of the simulated 3-layer model.

Table 1 summarizes all relevant parameters that are used for the simulations. The particle diameter value is kept constant as size variations mainly lead to different resonance amplitudes, following the arguments by Etrich et al. [30]. Note that the mesh's spatial resolution is set to 0.3 nm in and around the spheres. This high resolution was selected to assure good convergence of the solution.

Table 1. Summary of relevant simulations parameters

Parameter	Value
FDTD-simulation region	100 nm x 100 nm x 2000 nm
Boundary conditions	Bloch in X- and Y-direction. Perfect matching layer PML with 32 layers in z-direction
Mesh type, refinement and accuracy	Auto non-uniform, conformal variant 1 and level 5
Time step and minimum mesh size	dt stability factor 0.99 and 0.3 nm
Source	Linear polarized light in the X-Z-plane with bandwidth 300-800 nm. Injected at z = –800 nm with unit amplitude
Frequency domain power monitors	Transmission is recorded at z = 700 nm Reflection is recorded at z = –700 nm by subtracting the source's field from the measured one (most accurate)
Gold spheres	Constant diameter of 5 nm
Mirror layer	Spanning across the X-Y-plane Placed at Z = –90 nm, if not stated otherwise
Material parameters	Au (Gold) Johnson and Christy with 8 coefficients Al (Aluminum) CRC with 6 coefficients Ag (Silver) CRC with 6 coefficients All with 0.1 fit tolerance
Dielectric background and spacer	Constant value of 1.5
Early Shutoff	1E-6

3. Few particle systems

Understanding the mechanisms that lead to broadband absorption within the MIM system is essential for improving its performance and translating this concept to other systems. The experimentally fabricated system by Hedayati at al. consists of many randomly arranged gold nano particles above a gold mirror layer [25]. Investigations of such large random systems are presented in Section 4; let us however get some basic understanding by investigating the optical response of a few individual particles, which represent the ingredients of the large system.

To answer the question what microscopic parameters are most important for strong broadband absorption, we first study the response of a few particles with diameter 5 nm. This value is in good agreement with Hedayati's mean diameter of approximately 4.5 nm. The particles are embedded in a lossless dielectric medium of refractive index 1.5 and positioned 90 nm above a highly-reflective mirror layer, mostly a 100 nm thick gold layer. The single particles are placed within an arbitrarily sized region of 100 nm periodicity in x- and y-directions (simulations with a 200 nm period revealed no significant differences and we can assume that the periodic particle pairs have thus negligible coupling at 100 nm distance).

Optics EXPRESS

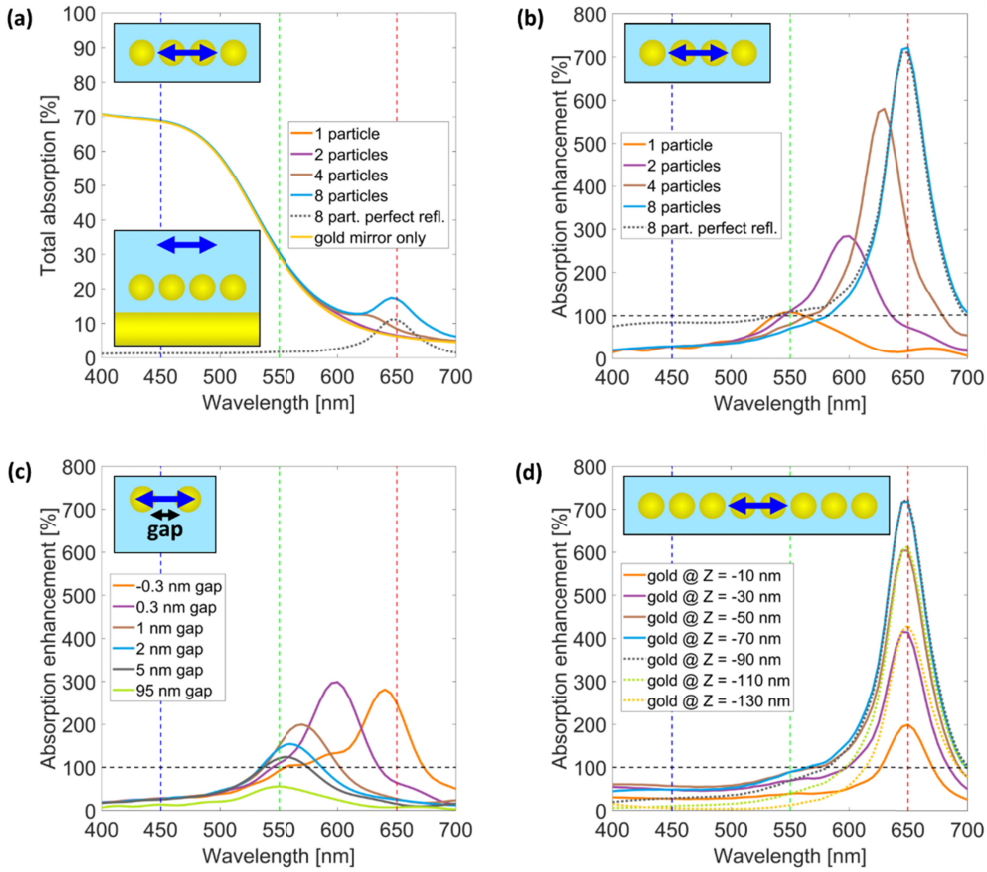

Fig. 2. (a) Total absorption for a 3-layer system with varying number of particles inside the top layer and (b) the corresponding absorption enhancement. (c) Absorption enhancement for varying gap sizes and (d) mirror particle distance. The top left insets show a simplified top view of the system, where the blue arrow marks the source's polarization and in (a), the bottom left inset shows a front view.

Figure 2(a) shows the total absorption of the system for various numbers of particles atop the gold mirror, while the center to center distance of 5.3 nm is kept constant. In the case of 8 particles, we also plot the total absorption of a system, where the gold mirror is replaced by a perfect reflector. In this simple case, it is obvious that the total absorption corresponds also to the absorption within the particles. The top left insets in Fig. 2 show a simplified top view of the modeled system, where the blue arrow indicates the source polarization. In Fig. 2(a), we also show a front view for a 4-particle system. The 3 colored vertical lines are selected wavelengths that represent the primary colors red, green and blue.

The second simple case is the "no particle"-case, where total absorption equals bulk absorption of the 100 nm thick gold layer and no energy is absorbed elsewhere. In all other cases it is less obvious where light is absorbed.

Figure 2(b) shows the rescaled absorption within the particles, which we call absorption enhancement and is defined in analogy to the absorption efficiency for the case of isolated particles [33],

$$\text{absorption enhancement}[\%] = A / G \cdot \text{particle absorption}[\%], \qquad (1)$$

where G denotes the particles' geometrical cross section projected on a plane, i.e. $G = n\pi a^2$ for n spherical particles of radius a and A is the simulation area. Equation (1) has the

Optics EXPRESS

advantage that the calculated absorption enhancement is independent of the somewhat arbitrarily chosen x-y-periodicity.

In contrast to the total absorption in Fig. 2(a), the absorption enhancement reported in Fig. 2(b) indicates how much light is absorbed at a specific wavelength within the particles. We see that the plasmon resonance red-shifts for increasing number of particles in Fig. 2(b) [34]. We also observe that the resonance strength dramatically increases and exceeds the geometrically possible absorption by a factor of 7. The enhancement in the blue and cyan parts of the spectrum remains however relatively low and nearly constant. Please note that this behavior is highly polarization sensitive. In the case of 90° rotated source polarization, the absorption enhancement is even reduced with increasing number of particles (data not shown).

Figure 2(c) shows the strong gap dependence of the absorption enhancement. The dimer's enhancement is maximal in the case of a negative gap and thus overlapping particles, where the absorption maxima is also most red-shifted. Increasing the gap reduces the enhancement and already at a gap of 2 nm, the enhancement is only about 50% stronger than in the case of isolated particles (95 nm gap). Therefore, we conclude that small gaps and overlapping particles are key for strongly enhanced and red-shifted absorption. This is in agreement with previous reports that the gap size must be smaller than 10% of the particles diameter to realize strong red-shifts and enhancements [35,36].

The strong enhancement could be a consequence of two different mechanisms; inter-particle coupling and plasmonic mode coupling of particles with the metallic mirror due to the small distances. The latter was investigated for example by Nordlander and Prodan for the case of a single particle atop a metallic mirror [37]. However, Fig. 2(d) shows that the hybridization of the modes is negligible here. The absorption enhancement of 8 particles is symmetric around a mirror distance of 80 nm. The range over which it is symmetric varies with the wavelength. Comparing for example the mirror distances 50 nm and 110 nm in Fig. 2(d) reveals that it is most symmetric around the resonance. This indicates that the strong absorption enhancement is mainly a consequence of enhanced resonances due to interference.

Actually, Li et al. realized nearly perfect absorption based on interference with an even simpler MIM system [38]. They used a thin and homogenous chromium layer atop a chromium mirror layer, separated by a 90-100 nm thick SiO_2 spacer layer. They experimentally achieved an average absorption greater than 95% in the VIS and clearly demonstrated that the high absorption is the result of their manufactured lossy Fabry-Perot cavity. Similar absorption performance can be achieved also for embedded systems, even at elevated temperatures [39,40]. Ghobadi et al. recently showed that one can even increase the bandwidth further by replacing the homogenous top layer with a multi-step one [41], while Ding et al. used two dielectric thin metal layer pairs to broaden and maximize absorption [42].

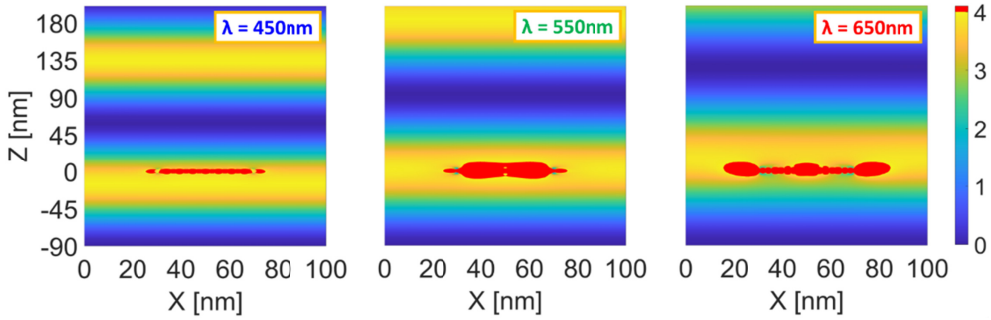

Fig. 3. Intensity distribution in the X-Z-plane at three different wavelengths λ for 8 gold particles embedded in a semi-infinite dielectric atop a perfect reflector, which is located at Z = –90 nm.

Optics EXPRESS

Both works agree with our finding that interference enhances absorption and in fact, simulations without gold mirror reveal that one needs almost 4 subsequent layers of 8 particles at 150 nm distance in light propagation direction to reproduce the strong enhancement (data not shown). This is another indication for interference as ideal 2 beam interference enhances intensity by a factor of four, which is here the case. Figure 3 shows that the intensity is certainly greater than 3 times the incident intensity at the location of 8 particles 90 nm above a perfect reflector. This makes sense despite the small distance of 90 nm, as the perfect reflector leads to a phase change of 180° and the 90 nm spacing to phase changes from 150° @ 650 nm to 216° @ 450 nm. These phase changes add up to almost 360° within the nano-composite layer, which is required for perfect constructive interference and we can conclude that the enhancement is also significantly influenced by lossy Fabry-Perot interference. Let us note that a similar phase phenomenon has recently been used to build ultrathin planar cavity metasurfaces by Wang et al. [43].

Although manufactured particles at single nanometer length scales tend to be spherical [15,18,25], let us for completeness also report on the response of other possible particle shapes. Figure 4(a) shows the absorption enhancement of a few spherical particles, which was reported in Fig. 2(b) and is included here for easy comparison with the other results. Figures 4(b)–4(d) show the absorption enhancement for three possible particle shapes; hemi-spheres, pillars and cubes, accounting in Eq. (1) for the different geometrical cross sections of these particle shapes. We find that other particle shapes lead to higher amplitudes compared to spherical ones. Note that this is also true if we normalize the data to the effective particle volumes.

For non-spherical particles, we also find that increasing the number of particles in a chain aligned with the source polarization leads to a red-shifted and strengthened resonance, as in the case of spherical particles. However, the resonance of a single non-spherical particle is already red-shifted compared to the spherical case and thus one would need to use different materials to absorb strongly in the VIS, especially in the blue and green part of the spectrum. This is an option that is explored in Section 4 for the case of spherical particles.

Optics EXPRESS

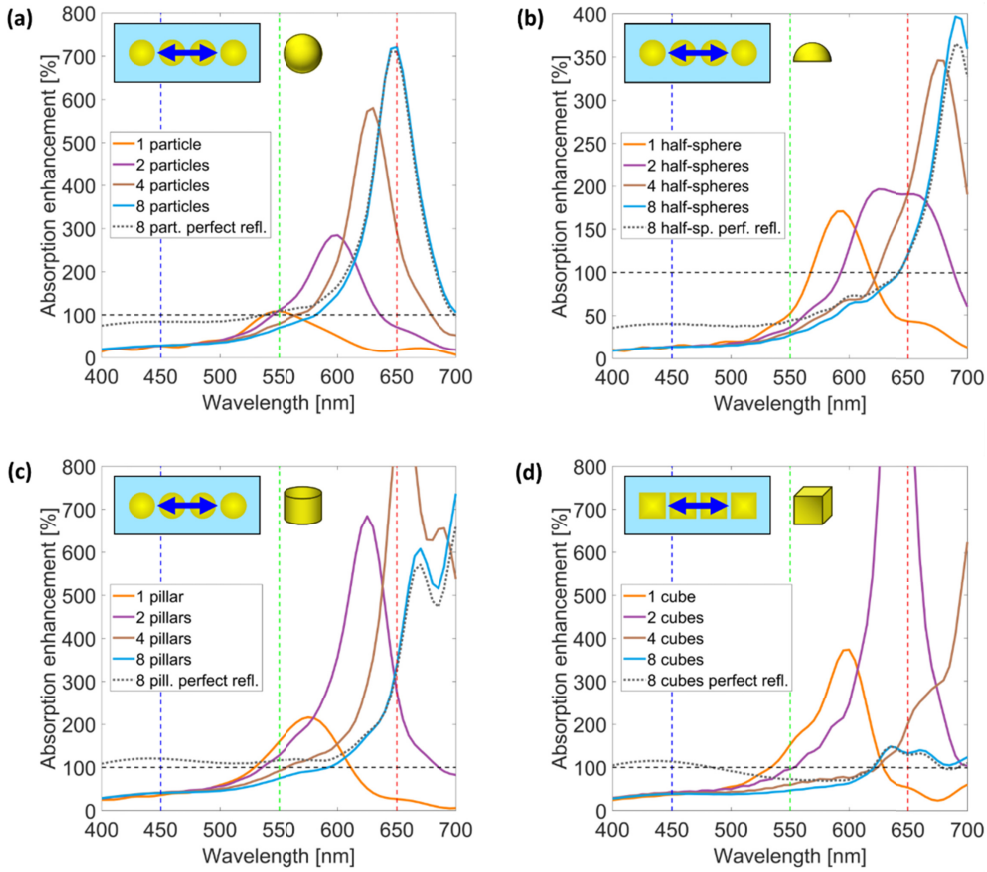

Fig. 4. (a) Absorption enhancement for a 3-layer system with varying number of spherical particles inside the top layer as reported in Fig. 2(b) and the enhancement for (b) hemi-spherical, (c) cylindrical (pillars) and (d) cubic particles. The top left insets show a simplified top view of the system next to a graphical visualization of the particle shape, where the blue arrow marks the source's polarization.

4. Many particle systems

Figure 2 reveals the absorption enhancement mechanisms for systems containing only a few well-ordered particles, while laboratory samples contain many unordered particles. To simulate the optical performance of these samples, we must include a mean of randomization. Several approaches to mimic randomization were evaluated and a system with densely and partially overlapping particles exhibited the most promising performances for achieving perfect absorption. In this approach, particles can overlap a maximum of 1 nm and are otherwise freely placed with the only restriction that particles are not allowed to cross the periodic boundaries. A representative part of this realization is shown in the insets of Fig. 5. Systems with up to 4 gold particle layers are simulated and 2 different reflector materials, gold and aluminum, are studied. The mirror-particle distance is chosen to be again 90 nm as it showed maximum absorption in the case of fully periodic particle layers.

Figure 5(a) shows that both 4-layer systems reach 100% absorption in the red part of the spectrum. The absorption enhancement is thus large enough in this region to reach saturation. However, Fig. 5(a) also shows that the aluminum mirror system's absorption is lower in the blue and green parts of the spectrum compared to the gold mirror ones. Still, these systems absorb on average almost equally well, especially above 450 nm. This is certainly unexpected as the bulk absorption of the aluminum layer is significantly lower than the gold layer one,

Optics EXPRESS

but can be explained by investing where light is absorbed in the system. To this end, we computed the absorption of the particles and of the mirror separately.

The ratio of particle layer absorption to total absorption is plotted in Fig. 5(b) and shows that for both mirror materials most energy is absorbed within the particle layers in the red part of the spectrum. However, the situation changes in the green part and is clearly different in the blue part of the spectrum, where particle absorption remains only high for the aluminum case. It is this higher particle absorption that compensates for the lower absorption of the aluminum mirror layer. Replacing the gold layer by an aluminum layer at little costs in terms of total absorption for the 4-layer case certainly helps realize the system on an industrial scale [33]. One could even additionally reduce the mirror thickness, since the average transmission across the VIS of a 50 nm thick aluminum layer is already smaller compared to that of a 100 nm thick gold layer.

The lack in absorption efficiency below 450 nm visible in Fig. 5(a) might be compensated by a proper particle material choice. We therefore study in the following, if one could increase absorption in this part of the spectrum by changing the particle material to either silver or aluminum. We select these materials as their plasmon frequencies are in the blue, respectively UV region of the spectrum [44]. Simulations of a few silver particles' absorption enhancement showed significantly increased absorption efficiency in the blue and green, see Fig. 6(a), compared to the one of a few gold particles shown in Fig. 2(b).

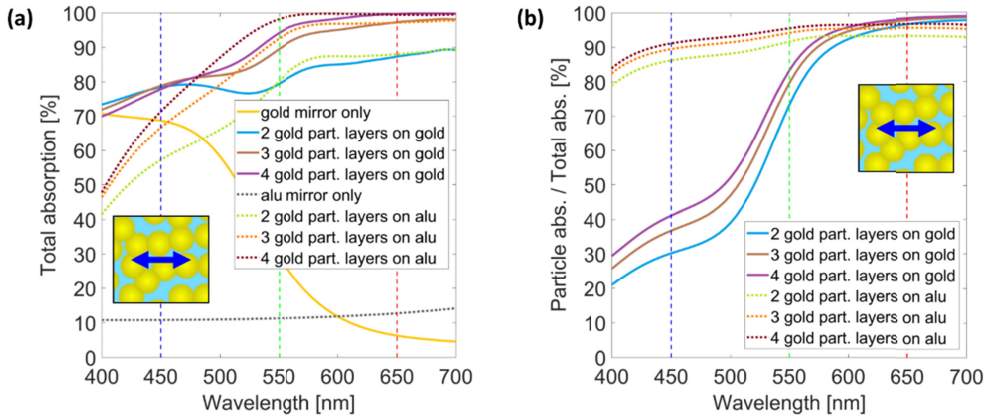

Fig. 5. (a) Total absorption of varying gold particles layers atop an aluminum or gold mirror layer and (b) the corresponding relative particle absorption fraction.

Figure 6(b) shows that in the case of aluminum particles, absorption can also be in enhanced in the blue, but significantly less in the green compared to silver. In both cases, absorption in the red region of the spectrum is lower compared to the gold particle case in Fig. 2(b). Thus, we mix gold particles with silver or aluminum particles in equal proportions to boost absorption in the blue/green thanks to the aluminum or silver particles' absorption behavior. To evidence the improvement provided by such a mixture, we study a system with only 3 particle layers to reduce absorption saturation in the red. Aluminum is selected as mirror layer material to clearly investigate the absorption effects related to the particle material choice and not due to the mirror layer material.

Figure 6(c) shows that mixtures of gold and silver particles (dotted orange line) as well as gold and aluminum particles (dotted dark red line) do indeed absorb more in the blue than the pure gold particle system (gold line). However, the systems containing only silver particles (light blue line) or aluminum particles (gray line) absorb even better than their corresponding mixtures with gold particles.

Given that the pure silver particle system absorbs even better in the blue than the pure aluminum one, we therefore surprisingly conclude that silver with its relatively low bulk

Optics EXPRESS

absorption is best for maximizing the system's total absorption in the visible part of the spectrum. Although this might be counterintuitive, this is in agreement with Etrich et al. [30]; it can also be understood by the fact that the silver absorption enhancement results show red-shifted and strongly enhanced absorption with increasing number of particles, see Fig. 6(a). It is remarkable that only 8 silver particles with 5.3 nm center-to-center distances achieve an absorption enhancement of almost 100% throughout the whole VIS. In Fig. 6(c), the system is much denser, and thus one can exploit this relative enhancement to increase also the total absorption to 100%. This exceptionally high absorption is a result of plasmonic inter-particle interaction and interference effects due to the 3-layer system. These two effects significantly boost the absorption rather than the silver's pure bulk material properties.

Please note that independent of the particle material choice, on average more than 93% of the light is absorbed within the particle layer, see Fig. 6(d). This in agreement with Li et al., who found that their ratio of thin film to mirror energy dissipation is larger by more than a factor of 15 for a lossy chromium Fabry-Perot configuration [38]. This shows again the similarity of both systems and the strong role played by interference.

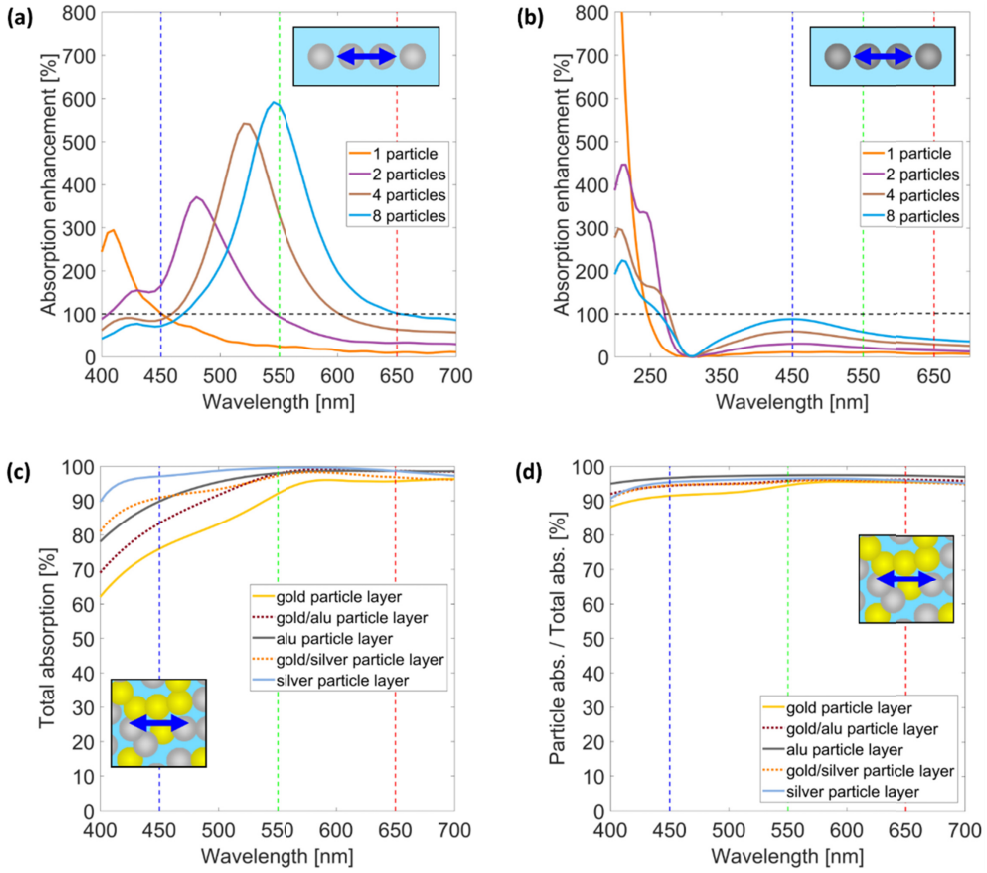

Fig. 6. (a) Absorption enhancement for a 3-layer system with varying number of silver particles and (b) varying number of aluminum particles inside the top layer atop an aluminum mirror layer. (c) Total absorption of 3 particle layers with varying material mixtures and (d) the corresponding relative particle absorption fraction.

Figure 6(d) shows that most of the light is absorbed within the particle layer, but not where it is absorbed locally. To answer this question, we calculate the local heat source density within the particle layers and integrate in z-direction. According to Baffou et al., the local heat source density $q(r_i)$ is defined as [45]:

Optics EXPRESS

$$q(r_i) = \omega\, Im(\epsilon)|E_i|^2, \tag{2}$$

where ω denotes the frequency, ϵ the total permittivity and $|E_i|^2$ the intensity at the location r_i within the particle. The local heat is a consequence of absorption and the local heat source density $q(r_i)$ is thus an indirect measure of local absorption.

Figure 7 shows the average $q(r_i)$ in z-direction for the three specific wavelengths that were marked in the figures above by colored vertical dashed lines. The average heat source density values were divided by 7000 J / s μm^2 and relative values exceeding one are plotted in red for easy comparison. In the case of 3 dense gold particle layers 90 nm above an aluminum mirror layer, one can observe three wavelength-dependent behaviors, see Fig. 7(a). In the blue at 450 nm, absorption within the particles is dominated by bulk material absorption and is thus mainly maximum in the center of the particles. In the green at 550 nm, one notices a transition from bulk to resonant absorption as edge and gap effects start to play a role. In the red at 650 nm, absorption is almost only determined by resonant effects at the particle edges just beneath their surface.

This agrees with the gold particles' absorption enhancement simulations, which showed reasonable resonant absorption enhancement in the green and strong enhancement in the red. Comparing qualitatively the results of Figs. 2(b) and 7(a) indicates that simulations of relatively simple few particle systems provide some understanding for the microscopic absorption behavior of the much more complex many particle systems.

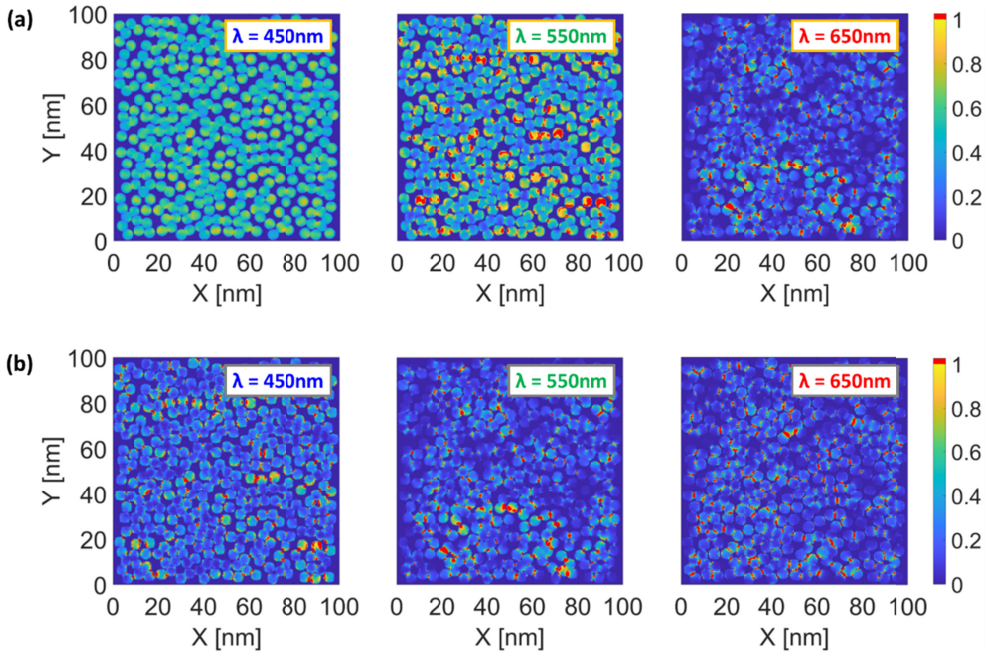

Fig. 7. Heat source density maps evaluated at three different wavelengths for MIM systems containing (a) 3 gold particle layers, or (b) 3 silver particle layers atop an aluminum mirror.

Figure 7(b) shows that the behavior is quite different in the case of 3 dense silver particle layers floating 90 nm above an aluminum mirror layer. Here, the absorption is determined mainly by resonant effects independent of the wavelength. This in agreement with our silver particles' absorption enhancement simulations in Fig. 6(a) that show great absorption enhancement throughout the VIS for varying number of particles.

Optics EXPRESS

5. Conclusion

We have investigated numerically the optical response of MIM systems with a top nano-composite layer and different mirror materials, particle materials and dielectric spacer thicknesses. We found that small gaps and overlapping particles are required for strong resonance enhancements within the nano-composite layer. In agreement with others, we found the resonance is red-shifted with increasing number of particles. Our data indicate that the distance of the composite layer to the mirror layer is of key importance as the MIM's high and broadband absorption is a consequence of lossy Fabry-Perot interference rather than a pure plasmonic effect. Consequently, interference strength can be maximized with highly reflecting mirror materials. Hence, systems with an aluminum mirror layer can maximize absorption despite their high reflectivity, while other highly reflecting materials would be equally suitable for that purpose.

Most of the light is resonantly absorbed within the particles, just beneath their surface. Thus, one can tune the absorption behavior by modifying particle material as shown here or by changing particle size or density. These results demonstrate the flexibility and versatility of MIM systems to absorb light efficiently over specific wavelength bands and the guidelines provided can assist one in realizing functionalities that require near-perfect absorption over specific wavelength bands.

Funding

European Research Council (ERC-2015-AdG-695206 Nanofactory).

References

1. S. V. Boriskina, T. A. Cooper, L. Zeng, G. Ni, J. K. Tong, Y. Tsurimaki, Y. Huang, L. Meroueh, G. Mahan, and G. Chen, "Losses in plasmonics: from mitigating energy dissipation to embracing loss-enabled functionalities," Adv. Opt. Photonics **9**(4), 775–827 (2017).
2. H. A. Atwater and A. Polman, "Plasmonics for improved photovoltaic devices," Nat. Mater. **9**(3), 205–213 (2010).
3. W. Zhang and O. J. F. Martin, "A universal law for plasmon resonance shift in biosensing," ACS Photonics **2**(1), 144–150 (2015).
4. W. Zhang, H. Fischer, T. Schmid, R. Zenobi, and O. J. F. Martin, "Mode-selective surface-enhanced Raman spectroscopy using nanofabricated plasmonic dipole antennas," J. Phys. Chem. C **113**(33), 14672–14675 (2009).
5. G. Lévêque and O. J. F. Martin, "Optical interactions in a plasmonic particle coupled to a metallic film," Opt. Express **14**(21), 9971–9981 (2006).
6. W. Zhu, F. Xiao, I. D. Rukhlenko, J. Geng, X. Liang, M. Premaratne, and R. Jin, "Wideband visible-light absorption in an ultrathin silicon nanostructure," Opt. Express **25**(5), 5781–5786 (2017).
7. K. Aydin, V. E. Ferry, R. M. Briggs, and H. A. Atwater, "Broadband polarization-independent resonant light absorption using ultrathin plasmonic super absorbers," Nat. Commun. **2**(1), 517 (2011).
8. F. Ding, J. Dai, Y. Chen, J. Zhu, Y. Jin, and S. I. Bozhevolnyi, "Broadband near-infrared metamaterial absorbers utilizing highly lossy metals," Sci. Rep. **6**(1), 39445 (2016).
9. T. Atay, J.-H. Song, and A. V. Nurmikko, "Strongly interacting plasmon nanoparticle pairs: from dipole–dipole interaction to conductively coupled regime," Nano Lett. **4**(9), 1627–1631 (2004).
10. J. Cesario, R. Quidant, G. Badenes, and S. Enoch, "Electromagnetic coupling between a metal nanoparticle grating and a metallic surface," Opt. Lett. **30**(24), 3404–3406 (2005).
11. Q. Chen, J. Gu, P. Liu, J. Xie, J. Wang, Y. Liu, and W. Zhu, "Nanowire-based ultra-wideband absorber for visible and ultraviolet light," Opt. Laser Technol. **105**, 102–105 (2018).
12. T. V. Teperik, V. V. Popov, and F. J. García de Abajo, "Void plasmons and total absorption of light in nanoporous metallic films," Phys. Rev. B Condens. Matter Mater. Phys. **71**(8), 085408 (2005).
13. N. Liu, M. Mesch, T. Weiss, M. Hentschel, and H. Giessen, "Infrared perfect absorber and its application as plasmonic sensor," Nano Lett. **10**(7), 2342–2348 (2010).
14. J. A. Bossard, L. Lin, S. Yun, L. Liu, D. H. Werner, and T. S. Mayer, "Near-ideal optical metamaterial absorbers with super-octave bandwidth," ACS Nano **8**(2), 1517–1524 (2014).
15. A. Leitner, Z. Zhao, H. Brunner, F. R. Aussenegg, and A. Wokaun, "Optical properties of a metal island film close to a smooth metal surface," Appl. Opt. **32**(1), 102–110 (1993).
16. U. K. Chettiar, P. Nyga, M. D. Thoreson, A. V. Kildishev, V. P. Drachev, and V. M. Shalaev, "FDTD modeling of realistic semicontinuous metal films," Appl. Phys. B **100**(1), 159–168 (2010).
17. T. Ji, L. Peng, Y. Zhu, F. Yang, Y. Cui, X. Wu, L. Liu, S. He, F. Zhu, and Y. Hao, "Plasmonic broadband absorber by stacking multiple metallic nanoparticle layers," Appl. Phys. Lett. **106**(16), 161107 (2015).

Optics EXPRESS

18. K. Seal, M. A. Nelson, Z. C. Ying, D. A. Genov, A. K. Sarychev, and V. M. Shalaev, "Growth, morphology, and optical and electrical properties of semicontinuous metallic films," Phys. Rev. B Condens. Matter Mater. Phys. **67**(3), 035318 (2003).
19. W. R. Holland and D. G. Hall, "Frequency shifts of an electric-dipole resonance near a conducting surface," Phys. Rev. Lett. **52**(12), 1041–1044 (1984).
20. M. Yan, J. Dai, and M. Qiu, "Lithography-free broadband visible light absorber based on a mono-layer of gold nanoparticles," J. Opt. **16**(2), 025002 (2014).
21. R. Yu, P. Mazumder, N. F. Borrelli, A. Carrilero, D. S. Ghosh, R. A. Maniyara, D. Baker, F. J. García de Abajo, and V. Pruneri, "Structural coloring of glass using dewetted nanoparticles and ultrathin films of metals," ACS Photonics **3**(7), 1194–1201 (2016).
22. K. J. Berean, V. Sivan, I. Khodasevych, A. Boes, E. Della Gaspera, M. R. Field, K. Kalantar-Zadeh, A. Mitchell, and G. Rosengarten, "Laser-induced dewetting for precise local generation of Au nanostructures for tunable solar absorption," Adv. Opt. Mater. **4**(8), 1247–1254 (2016).
23. H. Takele, H. Greve, C. Pochstein, V. Zaporojtchenko, and F. Faupel, "Plasmonic properties of Ag nanoclusters in various polymer matrices," Nanotechnology **17**(14), 3499–3505 (2006).
24. V. G. Kravets, S. Neubeck, A. N. Grigorenko, and A. F. Kravets, "Plasmonic blackbody: Strong absorption of light by metal nanoparticles embedded in a dielectric matrix," Phys. Rev. B Condens. Matter Mater. Phys. **81**(16), 165401 (2010).
25. M. K. Hedayati, M. Javaherirahim, B. Mozooni, R. Abdelaziz, A. Tavassolizadeh, V. S. K. Chakravadhanula, V. Zaporojtchenko, T. Strunkus, F. Faupel, and M. Elbahri, "Design of a perfect black absorber at visible frequencies using plasmonic metamaterials," Adv. Mater. **23**(45), 5410–5414 (2011).
26. J. Y. Lu, A. Raza, S. Noorulla, A. S. Alketbi, N. X. Fang, G. Chen, and T. Zhang, "Near-perfect ultrathin nanocomposite absorber with self-formed topping plasmonic nanoparticles," Adv. Opt. Mater. **5**(18), 1700222 (2017).
27. B. H. Choi, H.-H. Lee, S. Jin, S. Chun, and S.-H. Kim, "Characterization of the optical properties of silver nanoparticle films," Nanotechnology **18**(7), 075706 (2007).
28. S. Hewlett and A. Mock, "Engineering metamaterial absorbers from dense gold nanoparticle stacks," J. Appl. Phys. **122**(9), 093103 (2017).
29. M. K. Hedayati, F. Faupel, and M. Elbahri, "Review of plasmonic nanocomposite metamaterial absorber," Materials (Basel) **7**(2), 1221–1248 (2014).
30. C. Etrich, S. Fahr, M. K. Hedayati, F. Faupel, M. Elbahri, and C. Rockstuhl, "Effective optical properties of plasmonic nanocomposites," Materials (Basel) **7**(2), 727–741 (2014).
31. P. Feng, W.-D. Li, and W. Zhang, "Dispersion engineering of plasmonic nanocomposite for ultrathin broadband optical absorber," Opt. Express **23**(3), 2328–2338 (2015).
32. "http://www.lumerical.com/tcad-products/fdtd/," (2018).
33. C. F. Bohren and D. R. Huffman, *Absorption and Scattering of Light by Small Particles* (Wiley-VCH Verlag GmbH, 1998).
34. D. Brunazzo, E. Descrovi, and O. J. F. Martin, "Narrowband optical interactions in a plasmonic nanoparticle chain coupled to a metallic film," Opt. Lett. **34**(9), 1405–1407 (2009).
35. J. Kottmann and O. Martin, "Plasmon resonant coupling in metallic nanowires," Opt. Express **8**(12), 655–663 (2001).
36. H. Fischer and O. J. F. Martin, "Engineering the optical response of plasmonic nanoantennas," Opt. Express **16**(12), 9144–9154 (2008).
37. P. Nordlander and E. Prodan, "Plasmon hybridization in nanoparticles near metallic surfaces," Nano Lett. **4**(11), 2209–2213 (2004).
38. Z. Li, E. Palacios, S. Butun, H. Kocer, and K. Aydin, "Omnidirectional, broadband light absorption using large-area, ultrathin lossy metallic film coatings," Sci. Rep. **5**(1), 15137 (2015).
39. H. Deng, Z. Li, L. Stan, D. Rosenmann, D. Czaplewski, J. Gao, and X. Yang, "Broadband perfect absorber based on one ultrathin layer of refractory metal," Opt. Lett. **40**(11), 2592–2595 (2015).
40. M. Chirumamilla, A. S. Roberts, F. Ding, D. Wang, P. K. Kristensen, S. I. Bozhevolnyi, and K. Pedersen, "Multilayer tungsten-alumina-based broadband light absorbers for high-temperature applications," Opt. Mater. Express **6**(8), 2704–2714 (2016).
41. A. Ghobadi, S. A. Dereshgi, H. Hajian, B. Bozok, B. Butun, and E. Ozbay, "Ultra-broadband, wide angle absorber utilizing metal insulator multilayers stack with a multi-thickness metal surface texture," Sci. Rep. **7**(1), 4755 (2017).
42. F. Ding, L. Mo, J. Zhu, and S. He, "Lithography-free, broadband, omnidirectional, and polarization-insensitive thin optical absorber," Appl. Phys. Lett. **106**(6), 061108 (2015).
43. H.-C. Wang, C. H. Chu, P. C. Wu, H.-H. Hsiao, H. J. Wu, J.-W. Chen, W. H. Lee, Y.-C. Lai, Y.-W. Huang, M. L. Tseng, S.-W. Chang, and D. P. Tsai, "Ultrathin planar cavity metasurfaces," Small **14**(17), e1703920 (2018).
44. K. Thyagarajan, C. Santschi, P. Langlet, and O. J. F. Martin, "Highly improved fabrication of Ag and Al nanostructures for UV and nonlinear plasmonics," Adv. Opt. Mater. **4**(6), 871–876 (2016).
45. G. Baffou, R. Quidant, and C. Girard, "Thermoplasmonics modeling: A Green's function approach," Phys. Rev. B Condens. Matter Mater. Phys. **82**(16), 165424 (2010).